A Stochastic Geometry Analysis of Energy-Age Tradeoff in Wireless IoT Network

Songita Das, *Graduate Student Member*, *IEEE* and Gourab Ghatak, *Member*, *IEEE*
Bharti School of Telecommunications Technology and Management,
Indian Institute of Technology Delhi, New Delhi-110016, India
Email:bsz228102@iitd.ac.in, gghatak@ee.iitd.ac.in

***Abstract*—We investigate an internet of things (IoT) network where the IoT devices first leverage the received power from the transmitters for harvesting energy, and then employ the harvested energy to decode the data packets. In particular, we propose a slot division scheme based on a parameter ξ wherein the first phase of the slot is dedicated for energy harvesting (EH), while the second phase of the slot is dedicated for data transmission. We define a metric called the joint success probability (JSP) that jointly takes into account the event that the harvested energy exceeds an energy threshold and that the received signal to interference ratio (SIR) exceeds an SIR threshold. Deriving an exact expression for the JSP is challenging, and accordingly, we provide lower and upper bounds for the same. Based on this framework, we derive the peak age-of-information (PAoI) of the data packets. The higher the slot interval dedicated for EH, the lower will be the data transmission time, thereby requiring employment of a higher rate for a link. On the contrary, a lower slot interval allotted for the EH phase will result in the IoT devices not having sufficient energy to decode the packets successfully. We demonstrate that the optimal slot partitioning factor may be different for maximizing the JSP as compared to minimizing the PAoI. Accordingly, for different transmit powers and deployment areas, we recommend the optimal slot partitioning factor for the above two metrics.**

***Index Terms*—Radio-Frequency (RF), Joint Success Probability(JSP), Peak Age of Information (PAoI), Energy Harvesting (EH), Stochastic Geometry, Internet of Things (IoT).**

I. Introduction

A. Context and Motivation

THE age of information (AoI) is a metric used in communication networks to assess how quickly information reaches its destination in relation to when it was created at the source [1]. Contrary to classical wireless performance metrics such as throughput and delay that characterize data transfer efficiency, the AoI adequately takes freshness into account. This makes it attractive for system design in real-time internet of things (IoT) applications [2]. Additionally, the devices for such IoT applications often are battery-constrained, and regular battery replacements are infeasible. To alleviate this, energy harvested (EH) is a key solution that converts ambient energy into usable electrical power [3]. EH provides a supplemental or alternative power source, allowing devices to run independently and sustainably [4]. Since the wireless signals are repurposed for EH, often it has an adverse impact on the decoding of the received signals, and consequently, the AoI. Hence, the joint characterization and optimization of EH and the AoI in wireless networks is critical, and is the focus of this paper.

B. Literature Review

Abd-Elmagid *et al.* [5] provide a comprehensive overview of AoI and its variants, and their utility in designing freshness-aware IoT networks. They contrast the key differences of the AoI with respect to classical wireless network performance metrics such as throughput and delay. Furthermore, they reveal achievable AoI regions with optimal energy sampling and transmission policies. Yates and Kaul [6] analyzed AoI in queues for stochastic hybrid systems that utilize memoryless service. Indeed, AoI and its optimization has been the subject of extensive research in a variety of network scenarios in an effort to improve the freshness of data. Chen *et al.* [7] studied multi-hop wireless sensor nodes (WSNs) that employ EH while optimizing AoI. In particular, they formulate an NP-hard problem to minimize the same. Consequently, they propose an algorithm `MAoIG` and characterize the bounds on peak age of information (PAoI) and average AoI achieved by their algorithm. On the contrary, Zhu *et al.* [8] focused on the scheduling challenges associated with minimizing AoI in battery-free one-hop WSNs by employing a variety of EH strategies. In particular, the authors discuss the optimal offline policy and introduce competitive online policies for minimizing AoI. Zhang *et al.* [9] investigated the impact of deploying mobile edge computing (MEC) servers on the computational ability of the sensor nodes. They formulated a non-convex problem to optimize the sampling rate, computation rate, and the AoI, and proposed a successive convex approximation technique to solve the same. Kim *et al.* [10] investigated optimal duty cycles for self-sustaining operation. For further works on joint AoI and EH optimization, we refer the reader to the references [11]–[18].

Rigorous optimization procedures, although useful for specific network instances, do not provide insights on the variance of performance measures across different network realizations. In this regard, stochastic geometry provides useful tools for the statistical characterization of such networks, thereby enabling the derivation of key system-design insights and dimensioning rules. Leveraging stochastic geometry, Mankar *et al.* [19] study both preemptive and non-preemptive queuing and their impact on the AoI in large-scale wireless networks constituting source-destination pairs. In particular, they derive tight bounds

ISBN 978-3-903176-65-2 © 2024 IFIP

on the moments and spatial distribution of PAoI using a bipolar Poisson point process model, which are validated through numerical results. Abd-Elmagid *et al.* [20] investigate the joint transmission coverage and energy harvesting performance in a network with node locations modeled as a Poisson cluster process (PCP). They state that computing the distribution of shot noise processes associated with the PCP is challenging. Consequently, they prescribe approximations for the characterization of joint signal and energy coverage. Yang *et al.* [21] have analyzed the spatio-temporal performance of AoI by using queuing theory in conjunction with stochastic geometry. They showed that a decentralized scheduling policy reduces AoI through local observations. The suggested method adjusts radio access probabilities to accommodate traffic changes to reduce PAoI, and accommodate network expansion. Furthermore, they extended their investigation in [22] to show that the last-come, first-served (LCFS) order has a variable impact on AoI in relation to the deployment density, while the slotted ALOHA protocol does not reduce AoI at low packet arrival rates.

Very few studies [23], [24] have investigated EH and AoI together in uplink stochastic geometry frameworks, where source nodes perform EH. In [23], the authors have characterized the AoI performance of the users by considering their EH capabilities. Based on their formulation, they have optimized the channel access policy that minimizes the AoI. On the contrary, [24] have studied the distributional properties of AoI by assuming that the status packets and the energy packets arrive at the devices following a Poisson arrival process. This enhances our understanding of the statistics of the AoI along with EH capabilities. None of the existing works however, derive the efficacy of the EH process jointly with the AoI. In particular, when fewer transmit nodes are located in the network, this not only enhances the signal coverage due to limited interference, but also in reduces the ability of the users to effectively harvest energy. In order to jointly study this, we introduce the term called joint success probability (JSP) and investigate how the temporal resources can be partitioned in order to maximize either the JSP or minimize the PAoI.

C. Contributions

We consider an energy harvesting IoT network where the IoT devices operate with harvested energy from the transmitters of the network. Given that the devices have harvested sufficient energy, they attempt to decode the downlink transmissions for the BSs. Based on this system, we make the following contributions.

1) First, we derive the probability of the joint event that the harvested energy at the device exceeds an energy threshold and that the downlink signal to interference ratio (SIR) exceeds an SIR threshold. We term this as the JSP and it determines the ability of any device in the network to simultaneously harvest the necessary energy to operate and the ability to decode the downlink data. To the best of our knowledge, this joint characterization has not yet been studied in stochastic geometry frameworks.
2) In order to allot resources between the EH and the data transmission functionalities, we consider a slotted frame design. Next, based on the derived JSP and by considering the slotted frame, we characterize the PAoI at the IoT devices with respect to the frame partitioning factor ξ.
3) Interestingly, we show that the optimal ξ that maximizes the JSP may not be identical to the one that minimizes the PAoI. Following this, we derive several system design insights. For example, based on the application of interest, the value of ξ must be tuned appropriately. While for the PAoI, the optimal ξ remains relatively stable at a high value in order to have sufficient harvested energy, the same decreases considerably with respect to P_t when the metric of interest is JSP.

II. System Model and Problem Formulation

A. Network Geometry

We consider an IoT network wherein the IoT devices are served by their nearest transmitter. Let the locations of the IoT devices be denoted by s_n, $n \in \{1, \ldots, N\}$. The transmitter locations are denoted by r_k. The typical IoT device is denoted by s_1 while the location of the transmitter closest to the typical IoT device is denoted by r_1. The transmitter locations are modeled as a Poisson point process (PPP), Φ with intensity λ in a disk $\mathcal{B}(s_1, R)$ of radius R centered at s_1. The distances between the typical IoT device and the typical transmitter is represented by $d_1 = \|s_1 - r_1\|$ and the distances from the typical IoT device to any other transmitter is represented by $d_k = \|s_1 - r_k\|$.

B. Propagation Model

Let the transmit power multiplied by the path-loss constant for all the transmitters be P_t. Accordingly, the power received by the typical IoT device from the associated transmitter in the $j-$th slot is given by $P_{R_1} = P_t g_1^j d_1^{-\alpha}$ while the interference power is given by $P_{R_k} = P_t \sum_{k=2}^{K} g_k^j d_k^{-\alpha}$. The small-scale fading gains are assumed to be exponentially distributed and denoted by g_1^j for the typical transmitter and g_k^j for the $k-$th interfering transmitter. Due to the PPP assumption for the location of the interferers, K is a Poisson distributed random variable with parameter $\lambda \pi R^2$. Assume that each time slot is of duration τ, and is divided into two distinct phases: an EH phase of duration $\xi\tau$ and a data transmission phase of duration $(1-\xi)\tau$. During the EH phase, the IoT device harvests RF energy from the downlink transmissions of all the transmitters. While, during the data transmission phase the typical IoT device uses the harvested energy to decode the packet received from the typical transmitter.

Let E_1^j represent the energy harvested by the typical IoT device in the j^{th} time slot. It has two components: the desired signal and the interfering signals. Mathematically,

$$E_1^j = \xi\tau P_{R_1} = \eta\xi\tau P_t \left(g_1^j d_1^{-\alpha} + \sum_{k=2}^{K} g_k^j d_k^{-\alpha} \right). \quad (1)$$

where, η represent energy efficiency. The typical IoT device must harvest more than E_{th} amount of energy to be able to power its receiving circuitry and, hence, receive data successfully during the information reception phase.

Let Υ_1^j represent the SIR measured at the typical IoT device and it is the ratio of the signal power to the interference power received at s_1 in the j^{th} time slot. Mathematically,

$$\Upsilon_1^j = \frac{P_t g_1^j d_1^{-\alpha}}{\sum_{k=2}^{K} P_t g_k^j d_k^{-\alpha}}. \tag{2}$$

In order to successfully decode the data packet, the SIR at the typical IoT device must be greater than an SIR threshold β. Let the number of bits to be transmitted be given by σ during the $(1-\xi)\tau$ faction of the slot dedicated for data transmission. Furthermore, let the required data rate, R is given by $R = \frac{\sigma}{(1-\xi)\tau}$. From the Shannon-Hartley theorem, the maximum data rate is the channel capacity, i.e., $C = B\log_2(1+\Upsilon_1^j)$, where B is the bandwidth of the channel. Thus, for transmission success, we need $C > R$ or $\Upsilon_1^j > 2^{\frac{R}{B}} - 1$. Thus, we set our SIR threshold as $\beta = 2^{\frac{R}{B}} - 1$.

C. Performance Metrics of Interest

Our main metrics of interest are JSP and PAoI denoted by μ_ϕ and A_i, respectively.

Definition 1. *The JSP, μ_ϕ is defined as the probability of the joint event that the harvested energy exceed the energy threshold E_{th} and the downlink SIR exceeds the SIR threshold β. Mathematically,*

$$\mu_\phi = \mathbb{P}[E_1^j > E_{th}, \Upsilon_1^j > \beta]. \tag{3}$$

Definition 2. *The AoI $\Delta(t)$ at time slot t is defined as the time elapsed since the last received packet at the IoT device was generated at the transmitter. Let G_{t_i} and t_i denote the generation and reception time instants of the i^{th} packet packet at the transmitter and the IoT device, respectively. Mathematically,*

$$\Delta(t+1) = \begin{cases} \Delta(t)+1, & \text{if transmission fails} \\ t_i - G_{t_i} + 1, & \text{otherwise} \end{cases} \tag{4}$$

Thus, $\Delta(t)$ increases in a staircase fashion with time slots and drops upon reception of a new packet at the destination, to the total number of slots experienced by this new packet in the system. The typical IoT device experiences interference from other transmitters.

We assume a non-preemptive queuing model. Let the packets arrive at the transmitter following a Bernoulli process with probability λ_a at each time slot. On the arrival of a new packet, the transmitter attempts to send this packet to the IoT device at each consecutive time slots. Until the transmission is successful, newly arrived packets are dropped. Let $W_i = t_i - G_{t_i}$ denote the time slots required for successful transmission of the $i-$th arrived packet. On successful delivery of the packet at the IoT device, the transmitter admits new packets. Let V_i denote the time slots between the successful delivery of the $(i-1)$-th packet and the arrival of the $i-$th packet. Thus,

$$Y_i = W_i + V_i, \tag{5}$$

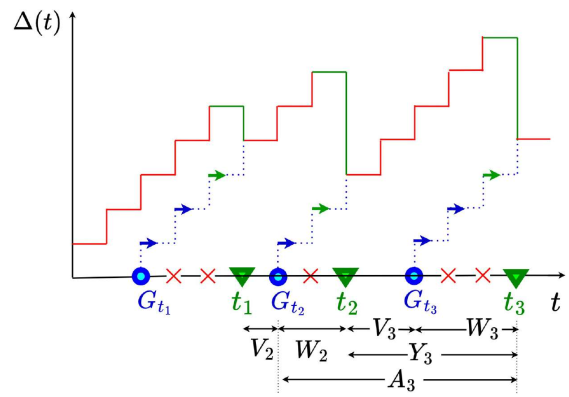

Fig. 1. Illustration of sample path of AoI

denotes the time elapsed between the successful delivery of the $(i-1)$-th and the i-th packet. In a given time slot both the EH and SIR at the typical IoT must surpass the E_{th} and β thresholds simultaneously for packet transmission to be successful, the probability of which is determined by μ_ϕ. Thus, given an arrival of a packet for transmission, the success event at each time slot is independent and identically distributed. Accordingly, the transmissions on a typical link can be represented using a Geo/Geo/1 model.

Fig. 1 depicts an AoI process sample path. Crosses indicate instances of packets being dropped during server activity of i^{th} packet trying to reach the destination. Then, the PAoI, A_i, corresponding to the $i-$th packet measures the maximum time elapsed since the last received, i.e., the $(i-1)-$th packet at the destination was generated. This is given by

$$A_i = W_{i-1} + Y_i. \tag{6}$$

III. Joint Success Probability Analysis

In this section, we analyze the performance of the proposed system model in terms of μ_ϕ. Since we focus on the impact of interference on the JSP, in what follows, we consider that at least two transmitters are located within the region of interest. Then, the following result characterizes the distances to the nearest and farthest transmitter.

Lemma 1. *Given that at least two point exists within the disc, the probability density function (PDF) of the farthest point in the disc is*

$$f_{d_K}(r) = \frac{2\lambda\pi r e^{-\lambda\pi\left(R^2 - r^2\right)}}{1 - \left(1+\lambda\pi R^2\right)e^{-\lambda\pi R^2}}, \quad r \geq 0, k \geq 2. \tag{7}$$

while, the PDF of the nearest point in the disc is as follows:

$$f_{d_1}(r) = \frac{2\lambda\pi r e^{-\lambda\pi r^2}}{1 - \left(1+\lambda\pi R^2\right)e^{-\lambda\pi R^2}}, r \geq 0. \tag{8}$$

Let us recall that the JSP is defined as the joint event that $E_1^j > E_{th}$ and $\Upsilon_1^j > \beta$. Substituting the value of the harvested energy and the SIR in equation (3) we get,

$$\mu_\phi = \mathbb{P}\left(g_1^j > d_1^\alpha\left[\frac{E_{th}}{\eta\xi\tau P_t} - \sum_{k=2}^{K} g_k^j d_k^{-\alpha}\right], g_1^j > \beta d_1^\alpha \sum_{k=2}^{K} g_k^j d_k^{-\alpha}\right). \tag{9}$$

The characterization of the above is challenging since it involves the derivation of the distribution of the sum of weighted exponential terms of the form $\sum_{k=2}^{K} g_k^j d_k^{-\alpha}$. Thus, obtaining the closed-form expression of μ_ϕ is infeasible. Consequently, we focus on deriving the upper bound $\mu_{\phi,U}$ and the lower bound $\mu_{\phi,L}$, of μ_ϕ. The idea behind the upper and the lower bounds of the JSP is as follows. If all the interfering transmitters are placed at the farthest location d_k in the disc, then energy harvested by the typical IoT is minimum. Similarly, if all the interfering transmitters are placed at the nearest location d_1 in the disc, then the energy harvested by the typical IoT is maximum. Let $E_1^{j,min}$ and $E_1^{j,max}$ denote the minimum and maximum harvested energy respectively. With the help of (1), we can write them as follows

$$E_1^{j,min} = \eta\xi\tau P_t \left(g_1^j d_1^{-\alpha} + d_K^{-\alpha} \sum_{k=2}^{K} g_k^j \right). \tag{10}$$

$$E_1^{j,max} = \eta\xi\tau P_t \left(g_1^j d_1^{-\alpha} + d_1^{-\alpha} \sum_{k=2}^{K} g_k^j \right). \tag{11}$$

where E_1^j is energy harvested by s_1 node in $\xi\tau$ time which is then used to keep s_1 node active such that it is able to read the desired transmitted signal from r_1 to s_1 in the remaining $(1-\xi)\tau$ time. Similarly, if all the interfering transmitters are placed in the same circumference as the signal transmitter i.e., at the nearest distance d_1 to the typical IoT, then this causes maximum interference to the typical IoT, hence SIR experienced by it is minimum and vice versa, as clear from the expression of SIR,

$$\Upsilon_1^{j,min} = \frac{P_t g_1^j d_1^{-\alpha}}{d_1^{-\alpha} \sum_{k=2}^{K} P_t g_k^j}. \tag{12}$$

$$\Upsilon_1^{j,max} = \frac{P_t g_1^j d_1^{-\alpha}}{d_K^{-\alpha} \sum_{k=2}^{K} P_t g_k^j}. \tag{13}$$

Accordingly, we can write $\mu_{\phi,L}$ and $\mu_{\phi,U}$ as $\mu_{\phi,L} = \mathbb{P}[(E_1^{j,min} > E_{th}), (\Upsilon_1^{j,min} > \beta)]$ and $\mu_{\phi,U} = \mathbb{P}[(E_1^{j,max} > E_{th}), (\Upsilon_1^{j,max} > \beta)]$. The analytical expression of $\mu_{\phi,L}$ and $\mu_{\phi,U}$ are given in Theorem 1 and Theorem 2, respectively.

Theorem 1. *The lower bound of μ_ϕ is given by*

$$\mu_{\phi,L} = \sum_{k=2}^{\infty} \Big[\int_{d_1=0}^{R} \int_{d_K=d_1}^{R} \int_{z=0}^{\frac{E_{th}}{\eta\xi\tau P_t(\beta d_1^{-\alpha} + d_K^{-\alpha})}} \left(\frac{z^{k-1}}{(k-1)!}\right) \exp\Big(\frac{-E_{th} d_1^{\alpha}}{\eta\xi\tau P_t} + d_1^{\alpha} d_K^{-\alpha} z - z\Big) f_{d_1}(r) f_{d_K}(r) f_K(k) \Big] d_z d_{d_K} d_{d_1} + \sum_{k=2}^{\infty} \Big[\int_{d_1=0}^{R} \int_{d_K=d_1}^{R} \int_{z=\frac{E_{th}}{\eta\xi\tau P_t(\beta d_1^{-\alpha} + d_K^{-\alpha})}}^{\infty} \left(\frac{z^{k-1}}{(k-1)!}\right) \exp(-\beta z - z) f_{d_1}(r) f_{d_K}(r) f_K(k) \Big] d_z d_{d_K} d_{d_1}, \tag{14}$$

where $f_K(k) = \frac{e^{-\lambda\pi R^2} (\lambda\pi R^2)^k}{k!}$ *and* $f_{d_1}(r)$ *and* $f_{d_K}(r)$ *are obtained from* (8) *and* (7).

Proof. A detailed proof is given in Appendix A. □

Theorem 2. *The upper bound of μ_ϕ is given by*

$$\mu_{\phi,U} = \sum_{k=2}^{\infty} \Big[\int_{d_1=0}^{R} \int_{d_K=d_1}^{R} \int_{z=0}^{\frac{E_{th}}{\eta\xi\tau P_t(\beta d_K^{-\alpha} + d_1^{-\alpha})}} \left(\frac{z^{k-1}}{(k-1)!}\right) \exp\Big(\frac{-E_{th} d_1^{\alpha}}{\eta\xi\tau P_t}\Big) f_{d_1}(r) f_{d_K}(r) f_K(k) \Big] d_z d_{d_K} d_{d_1} + \sum_{k=2}^{\infty} \Big[\int_{d_1=0}^{R} \int_{d_K=d_1}^{R} \int_{z=\frac{E_{th}}{\eta\xi\tau P_t(\beta d_K^{-\alpha} + d_1^{-\alpha})}}^{\infty} \left(\frac{z^{k-1}}{(k-1)!}\right) \exp(-\beta d_1^{\alpha} d_K^{-\alpha} z - z) f_{d_1}(r) f_{d_K}(r) f_K(k) \Big] d_z d_{d_K} d_{d_1}, \tag{15}$$

where, $f_K(k) = \frac{e^{-\lambda\pi R^2} (\lambda\pi R^2)^k}{k!}$ *and* $f_{d_1}(r)$ *and* $f_{d_K}(r)$ *are obtained from* (8) *and* (7).

Proof. A detailed proof is given in Appendix B. □

IV. PAoI ANALYSIS

The JSP influences the PAoI since it directly characterizes probability of success or failure in a given time slot. Recall that for the non-preemptive scenario, newly arriving packets at the transmitter are dropped until the one in transmission is successfully delivered. Based on the derived framework for JSP, the following Theorem characterizes an upper bound of the PAoI of the system.

Theorem 3. *The upper bound of the PAoI measured at the typical IoT device is*

$$A_{i,NP}^{U} = Z_a + \frac{2}{\mu_{\phi,L}}, \tag{16}$$

where lower bound of μ_ϕ gives an upper bound of the PAoI.

Proof. A detailed proof is given in Appendix C. □

We are interested in the upper bound of PAoI since the PAoI measures the maximum time elapsed since the last received packet at destination was generated, just before a new packet is received at destination. This gives a guarantee on the PAoI of the system. In the next section, first we validate and study the trends of the JSP and then investigate the optimal slot partitioning factor to optimize either the JSP or the PAoI.

V. SIMULATION RESULTS

In this section, we present simulation results to verify the derived expressions. Throughout this section, unless otherwise specified, we consider the system parameters as $E_{th} = 10$ mJ, $\alpha = 3$, $\sigma = 10$ bits, $\eta = 0.9$, $\xi = 0.4$, $\tau = 1$ sec, $\lambda = 0.003$ m^{-2}, $B = 10$ kHz, $R = 60$ m.

Fig. 2, shows that the lower bound of the JSP matches the actual value of JSP for lower values of transmit power, while it matches the corresponding upper bound for higher values of transmit power. On the contrary, we see from Fig. 3 that for a varied range of deployment area, the lower and the upper bounds closely follow the actual JSP. The JSP monotonically increases with the transmit power. This is because, with an increase in P_t, the harvested energy increases, while it has no impact on the SIR, where P_t appears both in the numerator and the denominator, and hence cancels out.

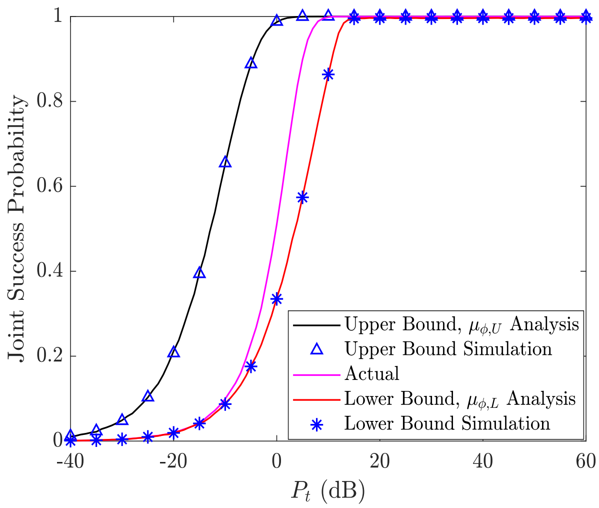

Fig. 2. The accuracy of the lower and upper bounds of the joint success probability, μ_ϕ with respect to the transmit power. Here $\tau = 10$ s.

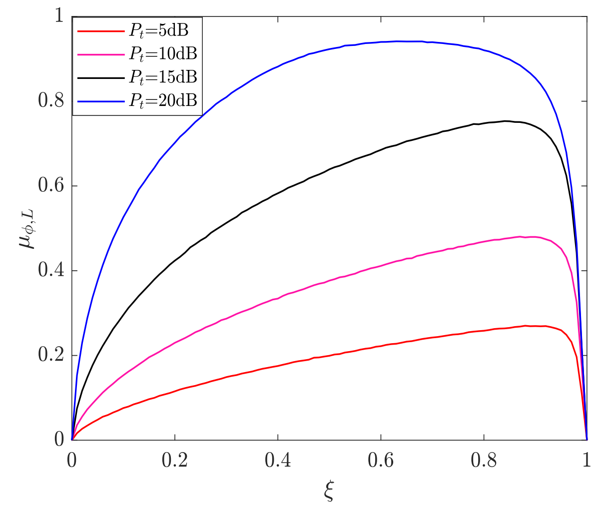

Fig. 4. Lower bound of joint success probability, $\mu_{\phi,L}$ with respect to fraction of time slot, ξ.

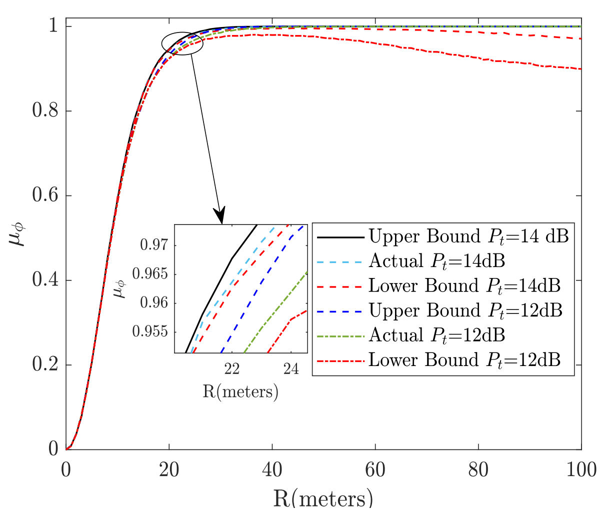

Fig. 3. Lower and upper bounds of joint success probability, μ_ϕ with respect to radius, R compared with the actual simulation.

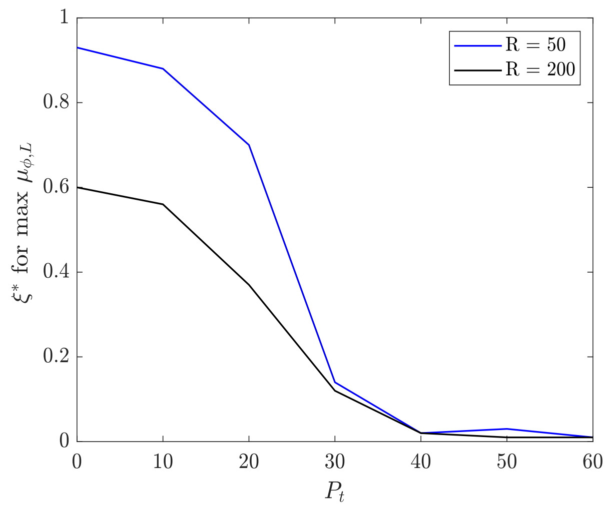

Fig. 5. Optimal slot partitioning, ξ^* for maximizing lower bound of joint success probability, $\mu_{\phi,L}$ with respect to transmit power, P_t.

Interestingly, with an increases of R the JSP first increases, reaches an optimal value and then decreases further. The initial increase is due to the enhancement in the harversted energy due to an increase in the number of transmitters. Albeit, this deteriorates the SIR, but for lower values of R, the SIR already exceeds its corresponding threshold. On the contrary, for larger values of R, the SIR deteriorates due to an increase in the number of interferers.

Fig. 4 and Fig. 6 confirm that when ξ is small, the IoT device does not harvest sufficient energy to be able to successfully decode the data packets in the data transmission phase, resulting in lower $\mu_{\phi,L}$ and higher $A^U_{i,NP}$. Similarly, when ξ is large, the data transmission interval is low, resulting in a higher link rate requirement. This degrades both $\mu_{\phi,L}$ and $A^U_{i,NP}$. This establishes the existence of an optimal slot partitioning factor ξ^* that maximizes JSP and minimizes PAoI, for a disc of a given radius, corresponding to each value of transmit power. This is clearly demonstrated in Fig. 5 and Fig. 7 respectively, for discs of varying radii. An interesting observation in Fig. 5 is that for larger values of R, as the radius of the disc increases, the number of interferers increase significantly thus decreasing SIR so the signal decoding time needs to be increased by decreasing the optimum charging phase duration in order to maximize JSP.

Both from Fig. 5 and Fig. 7 we can first observe that ξ^* for maximum JSP is different from ξ^* for minimum PAoI. Second, we can observe that as power transmitted increases, energy harvested also increases; thus, to further increase the maximum possible JSP, greater time can be allotted to information decoding, thereby decreasing ξ^*. In conclusion, ξ^* for lower values of transmit power is always greater than ξ^* values for higher values of transmit power.

Fig. 8 shows that when the transmit power is low, say $P_t = 5$ dB and the radius is very small, the number of interfering transmitters is also very less and barely grows with a small increase in the radius. At the same time, the signaling transmitter is very close to the receiver, so the

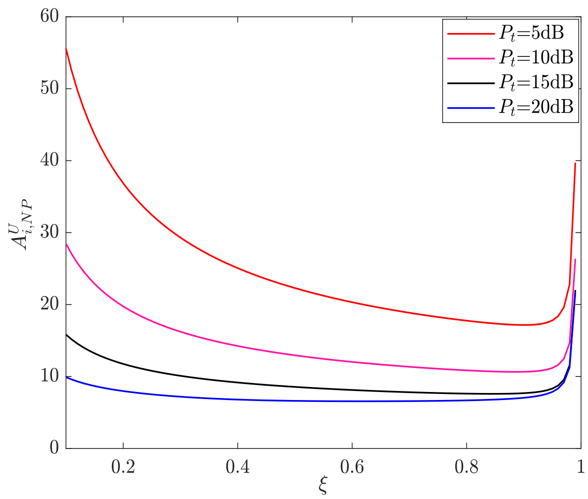

Fig. 6. Upper Bound of PAoI, $A^U_{i,NP}$ with respect to fraction of time slot, ξ.

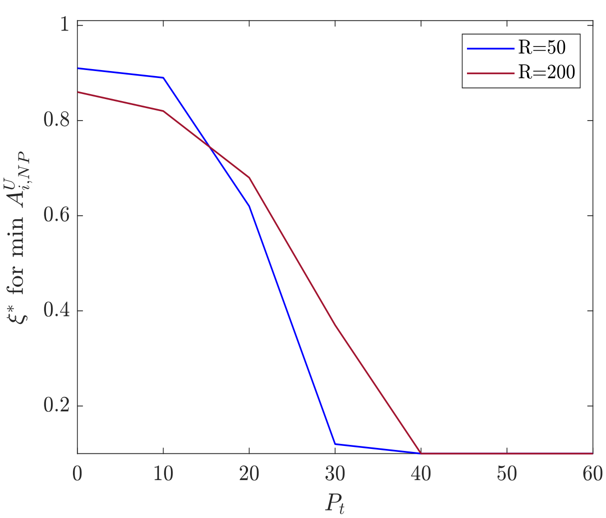

Fig. 7. Optimal slot partitioning, ξ^* for minimizing the upper bound of peak age of information, $A^U_{i,NP}$ with respect to transmit power, P_t.

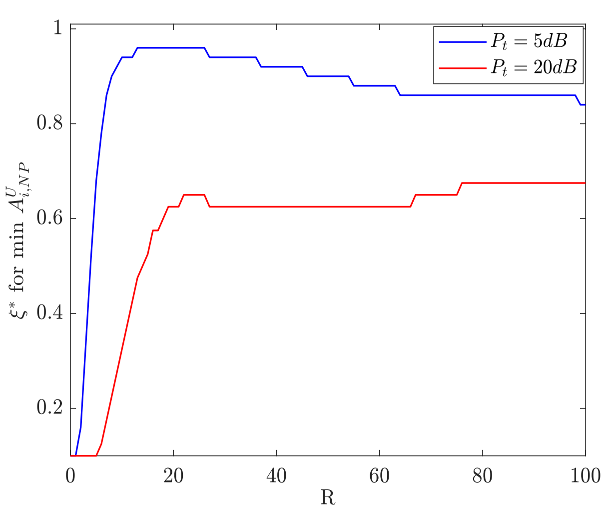

Fig. 8. Optimal slot partitioning, ξ^* for minimizing the upper bound of peak age of information, $A^U_{i,NP}$ with respect to radius, R.

SIR $> \beta$ threshold condition is easily met and the IoT device also harvests a small amount of energy, enough to meet the threshold, EH $> E_{th}$. However, with a small increase in the radius, the amount of energy harvested drops, therefore, EH time has to be increased by increasing ξ^* which maximizes JSP and minimizes PAoI.

At higher R values, as R increases, the number of interfering transmitters increase significantly. This means that excessive interference and insufficient signal power collectively hinder signal decoding, which in turn lowers the SIR. Thus, in order to maximize JSP and minimize PAoI, more time must be allocated for signal decoding, by decreasing ξ^*.

When the transmit power is high, say P_t = 20 dB and the radius is very small then with a small increase in the radius, ξ^* is increased for the same reason as previously stated; however, for larger R values, as R increases, the number of interferers increase significantly. Since stronger transmit power overcomes interference more efficiently, so the decrease in the SIR is not enough to hamper signal decoding, hence, more energy can be harvested by increasing ξ^* to further maximize JSP. This ensures that even with lesser time available for data transmission, the transmissions are successful a lot more often. This efficient use of higher transmit power allows JSP for higher values of transmit power to be greater than JSP for lower values of transmit power.

VI. Conclusion

This paper considered an IoT network where the IoT devices harvest energy from the power received from the transmitters and use it to decode the data packets. We then define and derieve the lower and upper bounds for the metric JSP and upper bound for the metric PAoI. Our analytical results show how time slot partitioning factor, disk radius, and other wireless network parameters affect JSP and PAoI. The key observations were that the optimal slot partitioning, ξ^* values for lower transmit power are always higher than those for higher transmit power. In low transmit power and small radius situations, ξ^* increases with a small increase in the radius while for large radius values, ξ^* decreases with increasing radius. When the transmit power is high and the radius is very small, then ξ^* increases with a small increase in the radius, but for large radius values, ξ^* increases again with increasing radius. Our numerical results indicate that the update arrival probability λ_a substantially impacts PAoI performance. As a promising avenue of future work, one can analyze protocols like ALOHA and CSMA-CD with a channel access parameter which can be optimized using some suitable RL algorithm.

Appendix A
Proof of Theorem 1

The lower bound of μ_ϕ is given as follows: $\mu_{\phi,L} = \mathbb{P}[(E_1^{j,min} > E_{th}), (\Upsilon_1^{j,min} > \beta)]$. Using (10) and (12), we can write $\mu_{\phi,L}$ as

$$\mu_{\phi,L} = \mathbb{P}\Bigg(g_1^j > \underbrace{d_1^{\alpha}\left[\frac{E_{th}}{\eta\xi\tau P_t} - d_K^{-\alpha}\sum_{k=2}^{K} g_k^j\right]}_{\Theta_1}, g_1^j > \underbrace{\beta\sum_{k=2}^{K} g_k^j}_{\Theta_2}\Bigg)$$

$$= \mathbb{P}\big(g_1^j > \max(\Theta_1, \Theta_2)\big)$$
$$= \underbrace{\mathbb{P}\big(g_1^j > \Theta_1, \Theta_1 > \Theta_2\big)}_{R_1} + \underbrace{\mathbb{P}\big(g_1^j > \Theta_2, \Theta_2 > \Theta_1\big)}_{R_2} \quad (17)$$

In the above expression, there are two probabilities that need to be solved. We solve them one by one. If $\Theta_1 > \Theta_2$, then we have $\big[E_{th}/\eta\xi\tau P_t - d_K^{-\alpha} Z > \beta d_1^{-\alpha} Z$, where $Z = \sum_{k=2}^{K} g_k^j$. To solve R_1, we have

$$R_1 = \mathbb{P}\left(g_1^j > d_1^{\alpha}\left[\frac{E_{th}}{\eta\xi\tau P_t} - Z d_K^{-\alpha}\right], Z < \frac{E_{th}}{\eta\xi\tau P_t\big[\beta d_1^{-\alpha} + d_K^{-\alpha}\big]}\right) \quad (18)$$

Let $t = d_1^{\alpha}\left[\frac{E_{th}}{\eta\xi\tau P_t} - Z d_K^{-\alpha}\right]$. If $t \geq 0 \Rightarrow Z \leq \frac{E_{th} d_K^{\alpha}}{\eta\xi\tau P_t}$. If $t < 0 \Rightarrow Z > \frac{E_{th} d_K^{\alpha}}{\eta\xi\tau P_t}$. The condition $t < 0$ will not occur since channel fading cannot be negative. Hence, we have

$$R_1 = \mathbb{P}\left(g_1^j > t, t > 0, Z < \frac{E_{th}}{\eta\xi\tau P_t\big[\beta d_1^{-\alpha} + d_K^{-\alpha}\big]}\right) \quad (19)$$

On substituting $t = d_1^{\alpha}\left[\frac{E_{th}}{\eta\xi\tau P_t} - Z d_K^{-\alpha}\right]$, we have

$$R_1 = \mathbb{P}\Bigg(g_1^j > d_1^{\alpha}\left[\frac{E_{th}}{\eta\xi\tau P_t} - Z d_K^{-\alpha}\right], \\ Z < \min\left(\frac{E_{th}}{\eta\xi\tau P_t\big[\beta d_1^{-\alpha} + d_K^{-\alpha}\big]}, \frac{E_{th} d_K^{\alpha}}{\eta\xi\tau P_t}\right)\Bigg) \quad (20)$$

Since, $\frac{E_{th}}{\eta\xi\tau P_t\left[\beta d_1^{-\alpha} + d_K^{-\alpha}\right]}$ is always less than $\frac{E_{th} d_K^{\alpha}}{\eta\xi\tau P_t}$. We can write

$$R_1 = \mathbb{P}\left(g_1^j > d_1^{\alpha}\left[\frac{E_{th}}{\eta\xi\tau P_t} - Z d_K^{-\alpha}\right], Z < \frac{E_{th}}{\eta\xi\tau P_t\big[\beta d_1^{-\alpha} + d_K^{-\alpha}\big]}\right)$$
$$= \mathbb{E}_Z\left\{\exp\left(-d_1^{\alpha}\left[\frac{E_{th}}{\eta\xi\tau P_t} - Z d_K^{-\alpha}\right], Z < \frac{E_{th}}{\eta\xi\tau P_t\big[\beta d_1^{-\alpha} + d_K^{-\alpha}\big]}\right)\right\}$$
$$= \int_0^{\frac{E_{th}}{\eta\xi\tau P_t\left[\beta d_1^{-\alpha} + d_K^{-\alpha}\right]}} \exp\left(-d_1^{\alpha}\left[\frac{E_{th}}{\eta\xi\tau P_t} - Z d_K^{-\alpha}\right]\right) f_Z(Z) dZ \quad (21)$$

The PDF of Z, $f_Z(Z)$ is as follows: $f_Z(Z) = \frac{e^{-Z} Z^{k-1}}{(k-1)!}$. Using $f_Z(Z)$ in(21), we get

$$R_1 = \int_0^{\frac{E_{th}}{\eta\xi\tau P_t\left[\beta d_1^{-\alpha} + d_K^{-\alpha}\right]}} \frac{Z^{k-1}}{(k-1)!} \\ \exp\left(-\left[\frac{E_{th} d_1^{\alpha}}{\eta\xi\tau P_t} - Z d_1^{\alpha} d_K^{-\alpha} + Z\right]\right) dZ \quad (22)$$

To Solve R_2, we can write

$$R_2 = \mathbb{P}\left(g_1^j > \beta Z, Z < \frac{E_{th}}{\eta\xi\tau P_t\big[\beta d_1^{-\alpha} + d_K^{-\alpha}\big]}\right)$$
$$= \mathbb{E}_Z\left\{\exp\big(-\beta Z\big), Z > \frac{E_{th}}{\eta\xi\tau P_t\big(\beta d_1^{-\alpha} + d_K^{-\alpha}\big)}\right\} \quad (23)$$
$$= \int_{\frac{E_{th}}{\eta\xi\tau P_t\left(\beta d_1^{-\alpha} + d_K^{-\alpha}\right)}}^{\infty} \exp\big(-\beta Z\big) f_Z(z) dZ$$

The PDF of Z, $f_Z(Z)$ is as follows: $f_Z(Z) = \frac{e^{-Z} Z^{k-1}}{(k-1)!}$. Using $f_Z(Z)$ in (23), we get

$$R_2 = \int_{\frac{E_{th}}{\eta\xi\tau P_t\left(\beta d_1^{-\alpha} + d_K^{-\alpha}\right)}}^{\infty} \exp\big(-\beta Z - Z\big) \frac{Z^{k-1}}{(k-1)!} dZ \quad (24)$$

Replacing (22) and (24) in (17) , we get (14).

APPENDIX B
PROOF OF THEOREM 2

Upper Bound of μ_ϕ is given as follows: $\mu_{\phi,U} = \mathbb{P}[(E_1^{j,max} > E_{th}), (\Upsilon_1^{j,max} > \beta)]$. Using (11) and (13), we can write μ_ϕ^U as

$$\mu_\phi^U = \mathbb{P}\Bigg(g_1^j > \underbrace{d_1^{\alpha}\left[\frac{E_{th}}{\eta\xi\tau P_t} - d_1^{-\alpha}\sum_{k=2}^{K} g_k^j\right]}_{\Theta_3}, g_1^j > \underbrace{\beta d_1^{\alpha} d_K^{-\alpha}\sum_{k=2}^{K} g_k^j}_{\Theta_4}\Bigg)$$
$$= \mathbb{P}(g_1^j > \max(\Theta_3, \Theta_4))$$
$$= \underbrace{\mathbb{P}(g_1^j > \Theta_3, \Theta_3 > \Theta_4)}_{R_1} + \underbrace{\mathbb{P}(g_1^j > \Theta_4, \Theta_4 > \Theta_3)}_{R_2}. \quad (25)$$

In the above expression, there are two probabilities that need to be solved. We solve them one by one. If $\Theta_3 > \Theta_4$ then we have $\Big[E_{th}/\eta\xi\tau P_t - d_1^{-\alpha} Z\Big] > \beta d_K^{-\alpha} Z$,where $Z = \sum_{k=2}^{K} g_k^j$. To solve R_1, we have

$$R_1 = \mathbb{P}(g_1^j > d_1^{\alpha}\left[\frac{E_{th}}{\eta\xi\tau P_t} - Z d_1^{-\alpha}\right], Z < \frac{E_{th}}{\eta\xi\tau P_t\big[\beta d_K^{-\alpha} + d_1^{-\alpha}\big]})$$

Let $t = d_1^{\alpha}\left[\frac{E_{th}}{\eta\xi\tau P_t} - Z d_1^{-\alpha}\right]$. If $t > 0 \Rightarrow Z < \frac{E_{th} d_1^{\alpha}}{\eta\xi\tau P_t}$ If $t < 0 \Rightarrow Z > \frac{E_{th} d_1^{\alpha}}{\eta\xi\tau P_t}$. The condition $t < 0$ will not occur since channel fading cannot be negative. Hence, we have

$$R_1 = \mathbb{P}\left(g_1^j > t, t > 0, Z < \frac{E_{th}}{\eta\xi\tau P_t\big[\beta d_K^{-\alpha} + d_1^{-\alpha}\big]}\right) \quad (26)$$

On substituting $t = d_1^{\alpha}\left[\frac{E_{th}}{\eta\xi\tau P_t} - Z d_1^{-\alpha}\right]$, we have

$$R_1 = \mathbb{P}\Bigg(g_1^j > d_1^{\alpha}\left[\frac{E_{th}}{\eta\xi\tau P_t} - Z d_1^{-\alpha}\right], \\ Z < min\left(\frac{E_{th}}{\eta\xi\tau P_t\big[\beta d_K^{-\alpha} + d_1^{-\alpha}\big]}, \frac{E_{th} d_1^{\alpha}}{\eta\xi\tau P_t}\right)\Bigg).$$

Since $\frac{E_{th}}{\eta\xi\tau P_t\left[\beta d_K^{-\alpha} + d_1^{-\alpha}\right]}$ is always less than $\frac{E_{th} d_1^{\alpha}}{\eta\xi\tau P_t}$. We can write

$$R_1 = \mathbb{P}\left(g_1^j > d_1^{\alpha}\left[\frac{E_{th}}{\eta\xi\tau P_t} - Z d_1^{-\alpha}\right], Z < \frac{E_{th}}{\eta\xi\tau P_t\big[\beta d_K^{-\alpha} + d_1^{-\alpha}\big]}\right)$$
$$= \mathbb{E}_Z\left\{\exp\left(-d_1^{\alpha}\left[\frac{E_{th}}{\eta\xi\tau P_t} - Z d_1^{-\alpha}\right], Z < \frac{E_{th}}{\eta\xi\tau P_t\big[\beta d_K^{-\alpha} + d_1^{-\alpha}\big]}\right)\right\}$$
$$= \int_0^{\frac{E_{th}}{\eta\xi\tau P_t\left[\beta d_K^{-\alpha} + d_1^{-\alpha}\right]}} \exp\left(-d_1^{\alpha}\left[\frac{E_{th}}{\eta\xi\tau P_t} - Z d_1^{-\alpha}\right]\right) f_Z(Z) dZ. \quad (27)$$

The PDF of Z, $f_Z(Z)$ is as follows: $f_Z(Z) = \frac{e^{-Z} Z^{k-1}}{(k-1)!}$. Using $f_Z(Z)$ in (27), we get

$$R_1 = \int_0^{\frac{E_{th}}{\eta\xi\tau P_t\left[\beta d_K^{-\alpha}+d_1^{-\alpha}\right]}} \exp\left(-\left[\frac{E_{th}d_1^{\alpha}}{\eta\xi\tau P_t}\right]\right)\frac{Z^{k-1}}{(k-1)!}dZ. \tag{28}$$

To Solve R_2, we can write

$$\begin{aligned} R_2 =& \mathbb{P}\bigg(g_1^j > \beta d_1^{\alpha} d_K^{-\alpha} Z, Z < \frac{E_{th}}{\eta\xi\tau P_t\left[\beta d_K^{-\alpha}+d_1^{-\alpha}\right]}\bigg) \\ =& \mathbb{E}_Z\bigg\{\exp\big(-\beta d_1^{\alpha} d_K^{-\alpha} Z\big), Z > \frac{E_{th}}{\eta\xi\tau P_t\big(\beta d_K^{-\alpha}+d_1^{-\alpha}\big)}\bigg\} \\ =& \int_{\frac{E_{th}}{\eta\xi\tau P_t\left(\beta d_K^{-\alpha}+d_1^{-\alpha}\right)}}^{\infty} \exp\big(-\beta d_1^{\alpha} d_K^{-\alpha} Z\big) f_Z(z) dZ. \end{aligned} \tag{29}$$

The PDF of Z, $f_Z(Z)$ is as follows: $f_Z(Z) = \frac{e^{-Z}Z^{k-1}}{(k-1)!}$. Using $f_Z(Z)$ in (29), we get

$$R_2 = \int_{\frac{E_{th}}{\eta\xi\tau P_t\left(\beta d_K^{-\alpha}+d_1^{-\alpha}\right)}}^{\infty} \exp\big(-\beta d_1^{\alpha} d_K^{-\alpha} Z - Z\big)\frac{Z^{k-1}}{(k-1)!}dZ. \tag{30}$$

Replacing (28) and (30) in (25), we get, (15)

Appendix C
Proof of Theorem 3

We can obtain $\mathbb{E}\big[W_i\big] = \sum_{n=1}^{\infty} n\big[\mu_{\phi,L}\big(1-\mu_{\phi,L}\big)^{n-1}\big]$. Replacing $1-\mu_{\phi,L} = t$, we get,

$$\mathbb{E}\big[W_i\big] = \sum_{n=1}^{\infty} n\big(1-t\big)t^{n-1} = \frac{1}{1-t} = \frac{1}{\mu_{\phi,L}}. \tag{31}$$

Similarly for V_i we can obtain $\mathbb{E}\big[V_i\big] = \sum_{n=0}^{\infty} n\big[\lambda_a\big(1-\lambda_a\big)^n\big]$. Replacing $1-\lambda_a = w$, we get,

$$\mathbb{E}\big[V_i\big] = \sum_{n=0}^{\infty} n\big(1-w\big)w^n = \frac{w}{1-w} \approx Z_a, \tag{32}$$

Thus, the upper bound of PAoI measured at the typical IoT is given by $A^U_{i,NP} = \mathbb{E}\big[A_i|(\beta, E_{th}) : \phi\big]$. From (5) and (6), $A^U_{i,NP} = \mathbb{E}\big[W_{i-1}\big] + \mathbb{E}\big[V_i\big] + \mathbb{E}\big[W_i\big]$. From (31) and (32), we get (16).

References

[1] R. D. Yates, Y. Sun, D. R. Brown, S. K. Kaul, E. Modiano, and S. Ulukus, “Age of information: An introduction and survey,” *IEEE Journal on Selected Areas in Communications*, vol. 39, no. 5, pp. 1183–1210, 2021.

[2] S. Kaul, R. Yates, and M. Gruteser, “Real-time status: How often should one update?” in *Proceedings IEEE INFOCOM*, 2012, pp. 2731–2735.

[3] X. Lu, P. Wang, D. Niyato, D. I. Kim, and Z. Han, “Wireless networks with RF energy harvesting: A contemporary survey,” *IEEE Communications Surveys and Tutorials*, vol. 17, no. 2, pp. 757–789, 2015.

[4] R. Kumar, M. Gupta, K. Agrawal, and S. Prakriya, “NOMA based multiuser uplink signalling with energy harvesting IoT nodes,” in *IEEE Region 10 Conference (TENCON)*, 2023, pp. 714–719.

[5] M. A. Abd-Elmagid, N. Pappas, and H. S. Dhillon, “On the role of age of information in the internet of things,” *IEEE Communications Magazine*, vol. 57, no. 12, pp. 72–77, 2019.

[6] R. D. Yates and S. K. Kaul, “The age of information: Real-time status updating by multiple sources,” *IEEE Transactions on Information Theory*, vol. 65, no. 3, pp. 1807–1827, 2019.

[7] K. Chen, F. Benkhelifa, H. Gao, J. A. McCann, and J. Li, “Minimizing age of information in multihop energy-harvesting wireless sensor network,” *IEEE Internet of Things Journal*, vol. 9, no. 24, pp. 25 736–25 751, 2022.

[8] T. Zhu, J. Li, H. Gao, Y. Li, and Z. Cai, “AoI minimization data collection scheduling for battery-free wireless sensor networks,” *IEEE Transactions on Mobile Computing*, vol. 22, no. 3, pp. 1343–1355, 2023.

[9] G. Zhang, C. Shen, Q. Shi, B. Ai, and Z. Zhong, “AoI minimization for WSN data collection with periodic updating scheme,” *IEEE Transactions on Wireless Communications*, vol. 22, no. 1, pp. 32–46, 2023.

[10] S. Kim, R. Vyas, J. Bito, K. Niotaki, A. Collado, A. Georgiadis, and M. M. Tentzeris, “Ambient RF energy-harvesting technologies for self-sustainable standalone wireless sensor platforms,” *Proceedings of the IEEE*, vol. 102, no. 11, pp. 1649–1666, 2014.

[11] A. Hentati, W. Jaafar, J.-F. Frigon, and W. Ajib, “Analysis of the interdelivery time in IoT energy harvesting wireless sensor networks,” *IEEE Internet of Things Journal*, vol. 8, no. 6, pp. 4920–4930, 2021.

[12] A. Arafa, J. Yang, S. Ulukus, and H. V. Poor, “Age-minimal transmission for energy harvesting sensors with finite batteries: Online policies,” *IEEE Transactions on Information Theory*, vol. 66, no. 1, pp. 534–556, 2020.

[13] B. Yao, H. Gao, Y. Zhang, J. Wang, and J. Li, “Maximum AoI minimization for target monitoring in battery-free wireless sensor networks,” *IEEE Transactions on Mobile Computing*, vol. 22, no. 8, pp. 4754–4772, 2023.

[14] M. Costa, M. Codreanu, and A. Ephremides, “On the age of information in status update systems with packet management,” *IEEE Transactions on Information Theory*, vol. 62, no. 4, pp. 1897–1910, 2016.

[15] J. Wang, X. Cao, B. Yin, and Y. Cheng, “Sleep–wake sensor scheduling for minimizing AoI-penalty in industrial internet of things,” *IEEE Internet of Things Journal*, vol. 9, no. 9, pp. 6404–6417, 2022.

[16] X. Sun, F. Zhao, H. H. Yang, W. Zhan, X. Wang, and T. Q. S. Quek, “Optimizing age of information in random-access poisson networks,” *IEEE Internet of Things Journal*, vol. 9, no. 9, pp. 6816–6829, 2022.

[17] A. Sinha and R. Bhattacharjee, “Optimizing age-of-information in adversarial and stochastic environments,” *IEEE Transactions on Information Theory*, vol. 68, no. 10, pp. 6860–6880, 2022.

[18] N. Hirosawa, H. Iimori, K. Ishibashi, and G. T. F. D. Abreu, “Minimizing age of information in energy harvesting wireless sensor networks,” *IEEE Access*, vol. 8, pp. 219 934–219 945, 2020.

[19] P. D. Mankar, M. A. Abd-Elmagid, and H. S. Dhillon, “Spatial distribution of the mean peak age of information in wireless networks,” *IEEE Transactions on Wireless Communications*, vol. 20, no. 7, pp. 4465–4479, 2021.

[20] M. A. Abd-Elmagid, M. A. Kishk, and H. S. Dhillon, “Joint energy and SINR coverage in spatially clustered RF-powered IoT network,” *IEEE Transactions on Green Communications and Networking*, vol. 3, no. 1, pp. 132–146, 2019.

[21] H. H. Yang, A. Arafa, T. Q. S. Quek, and H. V. Poor, “Optimizing information freshness in wireless networks: A stochastic geometry approach,” *IEEE Transactions on Mobile Computing*, vol. 20, no. 6, pp. 2269–2280, 2021.

[22] ——, “Spatiotemporal analysis for age of information in random access networks under last-come first-serve with replacement protocol,” *IEEE Transactions on Wireless Communications*, vol. 21, no. 4, pp. 2813–2829, 2022.

[23] O. M. Sleem, S. Leng, and A. Yener, “Age of information minimization in wireless powered stochastic energy harvesting networks,” in *2020 54th Annual Conference on Information Sciences and Systems (CISS)*, 2020, pp. 1–6.

[24] M. A. Abd-Elmagid and H. S. Dhillon, “Distributional properties of age of information in energy harvesting status update systems,” in *2021 19th International Symposium on Modeling and Optimization in Mobile, Ad hoc, and Wireless Networks (WiOpt)*, 2021, pp. 1–8.